Measurement Report: Effects of anthropogenic emissions and environmental factors on biogenic secondary organic aerosol (BSOA) formation in a coastal city of Southeastern China

Youwei Hong[a,b,c,d*], Xinbei Xu[a,b,c], Dan Liao[e], Taotao Liu[a,b,c],Xiaoting Ji[a,b,c], Ke Xu[a,b,d], Chunyang Liao[f], Ting Wang[g], Chunshui Lin[g], Jinsheng Chen[a,b,c*]

[a]Center for Excellence in Regional Atmospheric Environment, Institute of Urban Environment, Chinese Academy of Sciences, Xiamen, 361021, China

[b]Key Lab of Urban Environment and Health, Institute of Urban Environment, Chinese Academy of Sciences, Xiamen, 361021, China

[c]University of Chinese Academy of Sciences, Beijing, 100049, China

[d]School of Life Sciences, Hebei University, Baoding, 071000, China

[e]College of Environment and Public Health, Xiamen Huaxia University, Xiamen 361024, China

[f]State Key Laboratory of Environmental Chemistry and Ecotoxicology, Research Center for Eco-Environmental Sciences, Chinese Academy of Sciences, Beijing 100085, China

[g] Institute of Earth Environment, Chinese Academy of Sciences, Xi'an, 710061, China

*Corresponding author E-mail: Jinsheng Chen (jschen@iue.ac.cn); Youwei Hong (ywhong@iue.ac.cn)

Abstract:

To better understand the formation of biogenic secondary organic aerosol (BSOA), aerosol samples with a 4 h time resolution were collected during summer and wintertime in the southeast of China, along with on-line measurements of trace gases, aerosol chemical compositions, and meteorological parameters. The samples were analyzed by gas chromatography-mass spectrometry for $PM_{2.5}$-bound SOA tracers, including isoprene (SOA_I), α/β-pinene (SOA_M), β-caryophyllene (SOA_C), and toluene (ASOA). The average concentrations of total SOA tracers in winter and summer were 38.8 and 111.9 ng m^{-3}, respectively, with the predominance of SOA_M (70.1% and 45.8%), followed by SOA_I (14.0% and 45.6%), ASOA (11.0% and 6.2%) and SOA_C (4.9% and 2.3%). Compared to those in winter, the majority of BSOA tracers in summer showed significant positive correlations with Ox (O_3+NO_2) (r = 0.443～0.808), HONO (r = 0.299～0.601), ultraviolet (UV) (r = 0.382～0.588) –and temperature (T) (r = 0.529～0.852), indicating the influence of photochemical oxidation under relatively clean conditions. However, in winter, BSOA tracers were significantly correlated with $PM_{2.5}$ (r = 0.407～0.867), NO_3^- (r = 0.416～0.884), SO_4^{2-} (r = 0.419～0.813), and NH_3 (r = 0.440～0.757), attributed to the contributions of anthropogenic emissions. Major BSOA tracers in both seasons was linearly correlated with aerosol acidity (pH) (r = 0.421～0.752), liquid water content (LWC) (r = 0.403～0.876) and SO_4^{2-} (r = 0.419～0.813). The results indicated that acid-catalyzed reactive uptake onto sulfate aerosol particles enhanced the formation of BSOA. In summer, the clean air mass originated from the ocean, and chlorine depletion was observed. We also found that concentrations of the total SOA tracers was correlated with HCl (R^2 = 0.545) and chlorine ions (r = 0.280～0.639) –in $PM_{2.5}$, reflecting the contribution of Cl-initiated VOC oxidations to the formation of SOA. In winter, the northeast dominant wind direction brought continental polluted air mass to the monitoring site, affecting the transformation of BSOA tracers. This implied that anthropogenic emissions, atmospheric oxidation capacity and halogen chemistry have significant effects on the formation of BSOA in the southeast coastal area.

带格式的：字体颜色：自动设置

带格式的：字体颜色：自动设置

带格式的：字体颜色：自动设置

带格式的：字体颜色：自动设置

带格式的：上标

Keywords: SOA tracers; biogenic volatile organic compounds; anthropogenic pollutants; atmospheric oxidation capacity; coastal area

1. Introduction

Secondary organic aerosol (SOA) has attracted widespread scientific research~~ers~~ concerns, due to its potential impacts on climate change, human health and air quality (Shrivastava et al., 2017; Reid et al., 2018; Zhu et al., 2019; Wang et al., 2021b). Understanding the formation of SOA and assessing its relevance for environmental effects become an integral part of aerosol chemistry (Charan et al., 2019; Xiao et al., 2020; Palmer et al., 2022). However, due to its complex precursors and atmospheric physical or chemical processes, SOA prediction by air quality models remains highly uncertain (McFiggans et al., 2019). Therefore, it is necessary to better explore missed SOA sources and unknown SOA formation mechanisms.

SOA ~~was~~ is produced by the conversion of biogenic and anthropogenic volatile organic compounds (BVOCs and AVOCs) through complex homogeneous and heterogeneous reactions (Charan et al., 2019; Xiao et al., 2020; Mahilang et al., 2021). BVOCs are the main precursors of SOA on a global scale, while AVOCs are the predominant contributor to SOA in urban areas (Hallquist et al., 2009; Wang et al., 2021a). Recently, laboratory, field ~~observation~~ and modeling studies have shown that anthropogenic emissions greatly affect the formation of BSOA (Hoyle et al., 2011; Shrivastava et al., 2019; Zhang et al., 2019b; Zhang et al., 2019c; Mahilang et al., 2021; Xu et al., 2021). Anthropogenic air pollutants, such as NOx, SO_2, NH_3 and aerosols, could influence the conversion of BVOCs to the particulate phase and the production of nitrogen and sulfur compounds (Wang et al., 2020). NOx is one of the important drivers of SOA formation and yields during both daytime and nighttime through alternating the fate of peroxy radicals (RO_2·) (Sarrafzadeh et al., 2016; Newland et al., 2021). While ·OH dominates the photochemical oxidation of BVOC during daylight hours, and NO_3·becomes one of the main oxidants for biogenic SOA and organic

~~nitrates~~ nitrate formation at night. SO_2 also plays an important role in changing SOA formation from BVOC photooxidation and ozonolysis through sulfuric acid formation and acid-catalyzed heterogeneous reactions (Zhao et al., 2018; Zhang et al., 2019b; Xu et al., 2021). In addition, NH_3 and amines can affect the SOA yields and composition through both gas-phase and heterogeneous reactions, by reacting with sulfuric or nitric acid to generate secondary inorganic aerosols (SIA) (Ma et al., 2018; Liu et al., 2021; Lv et al.,2022). However, due to complex precursors and atmospheric processes, the combined effects of anthropogenic emissions and meteorological factors on the formation of SOA are not fully understood.

The coastal area of southeastern China is under the East Asian monsoon control, which cause an obvious alternation of polluted and clean air masses from continental and ocean area, respectively (Wu et al., 2019; Hong et al., 2021). Also, the local geographical environment, including relatively high humidity, dense vegetation and strong atmospheric oxidation capacity, provides a good chance to study the sources and formation mechanisms of SOA. In our previous studies, ground-based observations in a mountainous forest area of this region showed that BSOA tracers were the largest contributor to SOA, and the aerosols were highly oxidized (Hong et al., 2019). However, with the development of rapid urbanization, anthropogenic emissions will be of great significance on SOA formation (Liu et al., 2020). Halogen radicals (chlorine, bromine, iodine) have an important role in tropospheric oxidants chemistry and OA formation (Wang et al., 2021c). Therefore, it is necessary to investigate the sources and formation mechanisms of SOA in coastal urban areas, and so as to provide a scientific basis for the estimation of regional SOA budgets and $PM_{2.5}$ pollution control.

In this study, a continuous $PM_{2.5}$ sampling campaign with a 4 h time resolution was conducted in a coastal city of southeastern China during the winter and summertime period. Seasonal, diurnal variations and SOC contributions of SOA tracers were analyzed. Atmospheric process identified by SOA tracers in different seasons were further analyzed. ~~We also demonstrated the indications of SOA tracers for air pollution process.~~ Finally, the combined effects of anthropogenic emissions and major

带格式的：字体：（中文）宋体，字体颜色：自动设置
带格式的：字体：（中文）宋体，小四，字体颜色：自动设置
带格式的：字体：（中文）宋体，字体颜色：自动设置
带格式的：字体：（中文）宋体，小四，字体颜色：自动设置
带格式的：字体：（中文）宋体，字体颜色：自动设置

environmental factors on promoting SOA formation was discussed.

2. Materials and methods

2.1 Sample collection

The sampling was performed at the Institute of Urban Environment, Chinese Academy of Sciences (118.06° E, 24.61° N), which is located in a suburban area of Xiamen, a coastal city of southeastern China. Detailed information of the air monitoring supersite was described in our previous study (Hong et al., 2021). Briefly, time-resolved (00:00–08:00, 08:00–12:00, 12:00–16:00, 16:00–20:00, 20:00–24:00 CST – China Standard Time) $PM_{2.5}$ samples were collected on the rooftop of the station (about 70m above the ground). The sampling was carried out by using a high volume (1.05 m^3 min^{-1}) sampler (TH-1000C, Wuhan Tianhong, China) with a $PM_{2.5}$ inlet from 10 to 18 January, and from 5 to 14 July 2020. All samples were collected onto pre-baked (450 ◦C, 6 h) quartz fiber filters. Field blank samples were also collected. The sample filters were separately sealed in aluminum foil and stored in a freezer (−20 ◦C) prior to analysis.

2.2 SOA tracers analysis by GC/MS

The isoprene-derived SOA (SOA_I) tracers included 2 methyltetrols (MTLs: 2-methylthreitol (MTL1) and 2-methylerythritol (MTL2)), C5-alkene triols (cis-2-methyl-1,3,4-trihydroxy-1-butene, trans-2-methyl-1,3,4-trihydroxy-1-butene, and 3-methyl-2,3,4-trihydroxy-1-butene) and 2-methylglyceric acid (MGA). The monoterpene-derived SOA (SOA_M) tracers were composed of pinic acid (PA), pinonic acid (PNA), 3-hydroxyglutaric acid (HGA), 3-methyl-1,2,3-butanetricarboxylic acid (MBTCA), 3-hydro-4,4-dimethyglutaric acid (HDMGA), and 3-acetylglutaric acid (AGA). The β-caryophyllene-derived SOA (SOA_C) tracer was β-caryophyllenic acid (CA), the toluene-derived SOA (SOA_A) tracer was 2,3-Dihydroxy-4-oxopentanoic acid (DHOPA) and levoglucosan (LEV) as a tracer of biomass burning. Due to the lack of authentic standards, surrogate standards (including erythritol, malic acid, PA and citramalic acid) were used to compensate for unavoidable assay variance of SOA_I, SOA_M, SOA_C and SOA_A tracer in each sample during the pretreatment process,

148 respectively (Fu et al., 2009). However, inherent low volatility of isoprene SOA tracers
149 could cause the uncertainties of using the GC/MS method, and low-volatility oligomers
150 might break down into monomers, such as C5-alkene triols and 2-methyltetrols (Lopez-
151 Hilfiker et al., 2016; Hu et al., 2016). Therefore, quantifying the abundance of certain
152 SOA tracers remained a lot of uncertainties.

153 The analytical procedure of fifteen SOA tracers was published in our previous
154 studies (Hong et al., 2019; Liu et al., 2020). Briefly, the filter samples were
155 ultrasonically extracted with a mixture of dichloromethane and methanol (2:1, v/v) for
156 10 min three times. The mixed extracts were filtered with a PTFE filter (0.22 μm), and
157 dried with high purity N_2 (99.99%), and then derivatized with 60 μL of
158 N,O-bis-(trimethylsilyl) trifluoroacetamide (BSTFA) with 1% trimethylsilyl chloride
159 and 10 μL of pyridine at 70 °C for 3 h. At last, 140 μL of internal standard solution (^{13}
160 C n-alkane solution, 1.507 ng μ L^{-1}) was added into the samples. Then, relative response
161 factors (RRFs) of surrogate and internal standard were calculated to quantify the
162 targeted organic tracers in each sample. Details of SOA tracer's calculated
163 concentrations based on RRFs were presented in our previous studies (Hong et al., 2019;
164 Liu et al., 2020).

165 Fifteen SOA tracers were determined by GC-MSD (7890A/5975C, Agilent
166 Technologies, Inc., USA) with a DB-5 MS silica capillary column (i.d. 30×0.25 mm,
167 0.25 μm film thickness). 1 μL sample was injected with splitless mode and high purity
168 helium (99.999%) was used as carrier gas at a stable flow of 1.0 mL/min. The GC
169 temperature was initiated at 100 °C (held for 1 min) and then to 300 °C at 5 °C min^{-1},
170 and kept at 300 °C for 10 min. The operation mode is electron ionization (EI) mode of
171 70 ev. The method detection limits (MDLs) for erythritol and PNA were 0.01 and 0.02
172 ng m^{-3}, respectively. The recoveries of erythritol, PNA, malic acid, PA and citramalic
173 acid were 67±2%, 73±1%, 75±1%, 88±7% and 82±8%, respectively. SOA tracers were
174 not detected in the field blank samples.

175 *2.3 Observations in the air monitoring supersite*

176 Water-soluble inorganic ions (WSII) in $PM_{2.5}$ (Cl^-, SO_4^{2-}, NO_3^-, Na^+, K^+, NH_4^+,

Mg^{2+}, and Ca^{2+}) and gas pollutants (HCl, HONO, HNO_3, NH_3) were hourly measured using a monitoring device for aerosols and gases in ambient Air (MARGA 2080; Metrohm Applikon B.V.; Delft, Netherlands). Internal calibration was carried out using LiBr standard solutions. The detection limit of Cl^-, SO_4^{2-}, NO_3^-, Na^+, K^+, NH_4^+, Mg^{2+}, and Ca^{2+} were 0.01, 0.04, 0.05, 0.05, 0.09, 0.05, 0.06 and 0.09 μg m^{-3}, respectively.

Hourly mass concentrations of $PM_{2.5}$ and PM_{10} were measured by using a tapered element oscillating microbalance (TEOM1405, Thermo Scientific Corp., MA, USA). NO_2, SO_2, and O_3 were monitored using continuous gas analyzers (TEI 42i, 43i, and 49i, Thermo Scientific Corp., MA, USA). Ambient meteorological parameters including relative humidity (RH), temperature (T), wind speed (WS), and wind direction (WD) were obtained by an ultrasonic atmospherium (150WX, Airmar, the USA). Photolysis frequencies were determined using a photolysis spectrometer (PFS-100, Focused Photonics Inc., Hangzhou, China), including the photolysis rate constants *J* (O^1D), *J* (HCHO_M), *J* (HCHO_R), *J* (NO_2), *J* (H_2O_2), *J* (HONO), *J* (NO_3_M) and *J* (NO_3_R), and the spectral band ranged from 270 to 790 nm. Boundary layer height (BLH) based on ERA-5 reanalysis dataset was downloaded from the following link https://www.ecmwf.int/en/forecasts/datasets/reanalysis-datasets/era5.

2.4 Estimation of SOC using a tracer-based method

The fraction of SOC formed by the oxidation of monoterpene, isoprene, β-caryophyllene and toluene was estimated using a tracer-based method (Kleindienst et al., 2007; Hong et al., 2019). It is defined as [SOC] = $\sum$i[tri]/f_{SOC}, where [SOC] represents the mass concentration of SOC (μgC m^{-3}) and $\sum$i [tri] means the sum of the concentration of individual SOA tracer (μg m^{-3}). The carbon mass fractions (f_{SOC}) of monoterpene, isoprene, β-caryophyllene and toluene were 0.231±0.111, 0.155±0.039, 0.023±0.005 and 0.008±0.003, respectively, based on smog-chamber experimental data (Kleindienst et al., 2007).

2.5 Aerosol acidity and OH calculation

The forward mode of ISORROPIA II thermodynamic model was used to calculate

the aerosol acidity (pH) (Fountoukis and Nenes, 2007). ISORROPIA II can calculate liquid water content (LWC), based on total SO_4^{2-}, NO_3^- (gas HNO_3 plus particle NO_3^-), Cl^-, ammonia (gas NH_3 plus particle NH_4^+), non-volatile cations (Na^+, K^+, Ca^{2+}, Mg^{2+}), and meteorological factors (RH and T) (Rumsey et al., 2014; Guo et al., 2016). The pH value from ISORROPIA II was calculated using the following equation:

$$pH = -\lg\left(\frac{1000 \times H^+}{LWC}\right)$$

where H^+ is the hydronium ion concentration loading for an air sample (μg/m^3).

The OH concentration ([OH]) was estimated using the NO_2 and HONO concentrations and the photolysis rate constants (J) of NO_2, O_3, and HONO, according to the following improved empirical formula (Wen et al., 2019).

$$[OH] = 4.1 \times 10^9 \times \frac{J(O^1D)^{0.83} \times J(NO_2)^{0.19} \times (140 \times NO_2 + 1) + HONO \times J(HONO)}{0.41 \times NO_2^2 + 1.7 \times NO_2 + 1 + NO \times k_{NO+OH} + HONO \times k_{HONO+OH}}$$

2.6 Statistical analysis

Correlation analysis by SPSS 22.0 software (IBM, Armonk, NY, USA) was used to study the relationship among SOA tracers, meteorological parameters and criteria air pollutants. One-way analysis of variance (ANOVA) was adopted to examine the variations of different factors.

2.7. Backward trajectory analysis

Hybrid Single-Particle Lagrangian Integrated Trajectory (HYSPLIT) was used to analyze the impacts of air masses on Xiamen during different seasons. 72 h backward trajectories were calculated every hour at a height of 500 m. The meteorological data with a resolution of 1° longitude × 1° latitude was obtained from the NCEP/GDAS. Cluster analysis was adopted using the total spatial variance (TSV).

3 Results and discussion

3.1. Overview of air pollutants

The concentrations of criteria air pollutants, including SO_2, CO, NO_2, O_3, $PM_{2.5}$ and PM_{10}, and meteorological parameters during wintertime and summertime were shown in Fig.1. The concentrations of $PM_{2.5}$ in winter ranged from 14.9 to 75.3 μg m^{-3}

with an average of 42.1 μg m^{-3}, which was much higher than that (the average of 18.4 μg m^{-3}) in summer, ranging from 12.8 to 46.4 μg m^{-3}. The concentrations of CO, NO_2 and PM_{10} showed similar seasonal trends to the pattern of $PM_{2.5}$. In contrast, O_3 had the highest concentration in summer, which was attributed to the formation of photochemical reaction under strong UV radiation and the weak titration of nitrogen oxides. Meanwhile, the concentrations of SO_2 (8.37±0.79 μg m^{-3}) in summer was also higher than that (2.63±1.95 μg m^{-3}) in winter, mainly attributed to the influence of coal combustion and ship emissions. The monitoring site was located approximately 15 km away from Xiamen port area and a coal-fired power plant (4 × 300 kW) in the south. Southerly winds were prevailed in summer, which might cause the relative high concentration of SO_2 in the monitoring site.

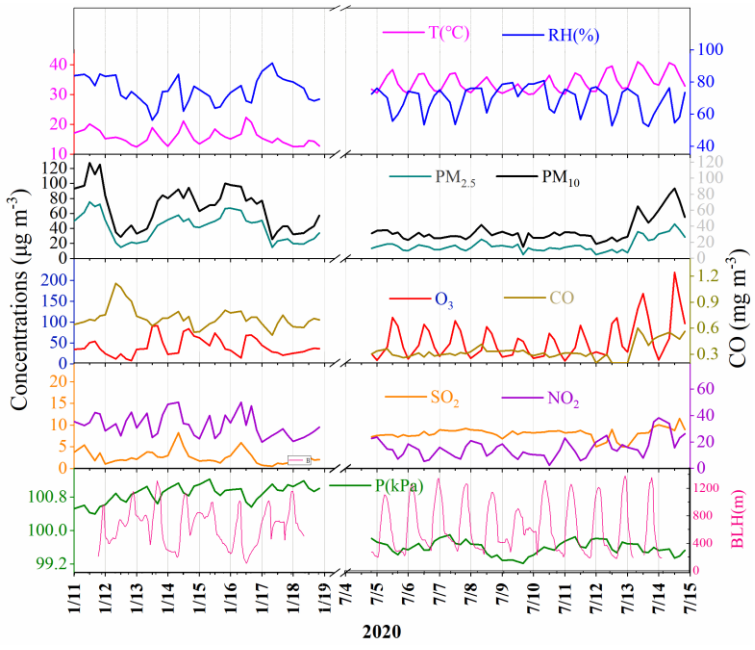

Figure 1. Time series of criteria air pollutants and meteorological parameters during the sampling period

3.2 Temporal variations of SOA tracers and estimated *SOC*

Temporal variations of individual SOA tracer are shown in Fig.S1. The average

concentrations of total SOA tracers in winter and summer were 37.3 and 111.3 ng m^{-3}, respectively. The predominance of SOA_M (26.6 ng m^{-3}), followed by ASOA (4.60 ng m^{-3}), SOA_I (4.35 ng m^{-3}) and SOA_C (1.76 ng m^{-3}) was observed in winter while SOA_I (54.4 ng m^{-3}) and SOA_M (47.8 ng m^{-3}) in summer were the main contributors to total SOA tracers, followed by ASOA (6.64 ng m^{-3}) and SOA_C (2.45 ng m^{-3}). In summer, BSOA tracers showed much higher concentrations in the daytime (149.3 ng m^{-3}) than in the nighttime (60.1 ng m^{-3}), while inverse results were observed in winter (30.4 ng m^{-3} and 35.0 ng m^{-3} in the daytime and nighttime, respectively). As shown in Table S2, in summer, SOA_I in the daytime ranged from 21.3 to 293.2 ng m^{-3} (average of 82.0±66.2 ng m^{-3}) and the concentrations of SOA_I ranging from 6.81 to 110.1 ng m^{-3} (average of 26.8±24.6 ng m^{-3}) were observed in the nighttime. However, in winter, the concentrations of isoprene SOA tracers in the daytime ranging from 1.36 to 11.1 ng m^{-3} (average of 3.79±2.37ng m^{-3}) were lower than those (average of 4.91±3.75 ng m^{-3}) in the nighttime. As shown in Fig. 2, diurnal variations of SOA_M, SOA_I, CPA and DHOPA tracers in summer showed high levels in the afternoon (12:00–16:00 CST), due to the impacts of beneficial photochemical oxidation conditions caused by high temperature and strong UV radiation. The related SOA tracers were consisted with the emissions of their precursors including biogenic and anthropogenic VOCs, similar to our previous studies (Hong et al., 2019; Liu et al., 2020). However, the SOA tracers in winter showed the lowest concentrations in the morning (8:00–12:00 CST), related with the favorable dispersion conditions caused by the increasing planetary boundary layer height (BLH) (Fig.1). Levoglucosan (LEV), a typical tracer of biomass burning, similar seasonal and diurnal trend to other tracers was observed. However, LEV may not be as stable in the atmosphere, especially under high relative humidity conditions (Hoffmann et al., 2010). In this study, maybe, it's hard to reflect the real concentration of LEV. A correlation of CPA with LEV was carried out (Fig.S2), just to discuss the impacts of biomass burning on the distribution of CPA tracers through local or long-range transport. Totally, high concentrations of BSOA tracers was found in the daytime and in summer, indicating the effects of temperature on biogenic VOCs emissions and their photochemical

oxidations. And the concentrations of BSOA tracers in winter increased in the nighttime, due to the changing of nocturnal boundary layer.

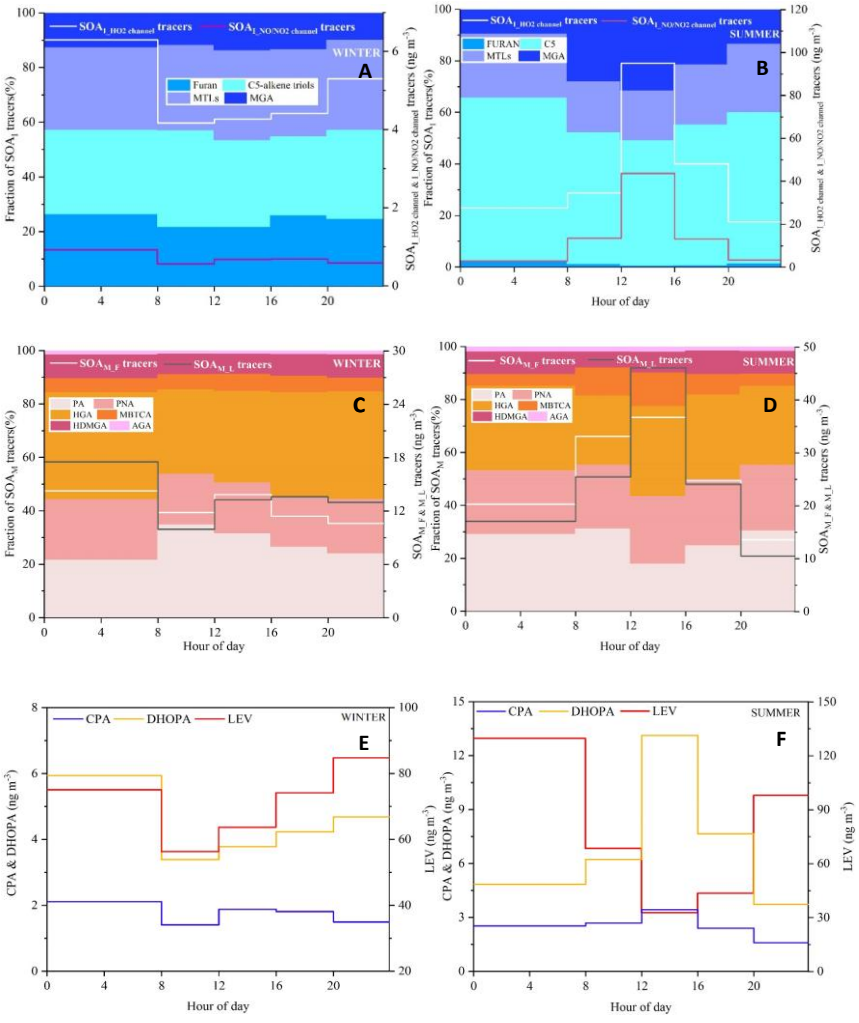

Figure 2. Diurnal variation of individual SOA tracer during the wintertime (A, C, and E) and summertime (B, D, and F)

As shown in Fig.~~3a~~S2a, b, SOA tracers-based SOC in winter and summer was estimated. ~~The concentrations of SOC in winter ranged from 0.27 to 2.36 μg C m^{-3}, with an average of 1.11 μg C m^{-3}. Meanwhile, the concentrations of SOC in summer ranged~~

~~from 0.46 to 7.85 μg C m^{-3}, with an average of 2.27 μg C m^{-3}.~~ The concentrations of SOC in summer was higher than that in winter, attributed to the increase of flourishing vegetation emissions and photochemical reactions under high temperature and strong solar radiation conditions. For individual SOA tracer, the concentrations of monoterpene-derived SOC ~~(0.87±0.64 μg C m^{-3})~~ was comparable to the toluene-derived SOC ~~(0.90±0.69 μg C m^{-3})~~, which were higher than isoprene-derived SOC ~~(0.39±0.38 μg C m^{-3})~~ and β-caryophyllene-derived SOC ~~(0.10±0.08 μg C m^{-3})~~. An obvious trend of diurnal variations of isoprene-derived SOC in summer was observed, which was consistent with the diurnal pattern of isoprene concentration (Fig.S3). However, no similar trend was found in winter, attributed to the influence of low temperature on inhibiting the emissions of isoprene from various kinds of plants. In addition, the toluene, monoterpene, isoprene and β-caryophyllene-derived SOC in summer accounted for 40.0%, 39.2%, 15.7% and 5.1% of the total SOC, respectively (Fig.~~3c~~S2c, d). However, in winter, the percentages of toluene, monoterpene, isoprene and β-caryophyllene-derived SOC were 47.2%, 42.1%, 3.2% and 7.6%, respectively. The percentages of isoprene-derived SOC estimated from different precursors varied significantly among the seasons. High temperature enhanced the emissions of isoprene, and strong solar radiation favored the formation of isoprene SOA tracers, contributing to the highest isoprene-derived SOC percentage in summer (Ding et al., 2014). And the highest percentages of toluene-derived SOC (47.2%) in winter were related with anthropogenic emissions and adverse diffusion conditions.

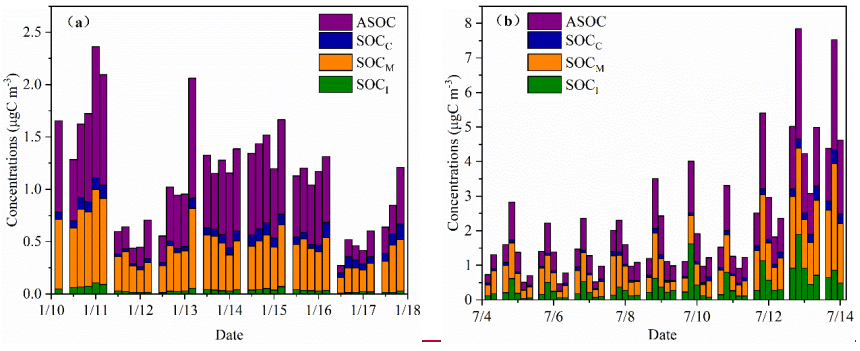

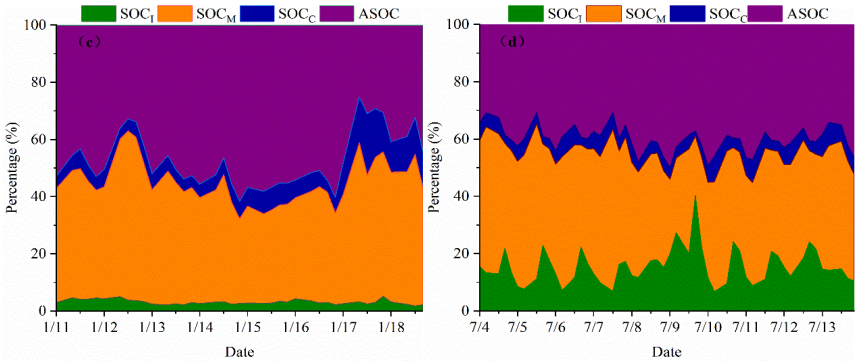

~~**Figure 3. Concentrations and percentages of SOA tracer-based estimated SOC during the sampling period**~~

3.3 Atmospheric process indication of BSOA tracers

As shown in Fig.~~4~~3, percentages of different types of SOA tracers in winter and summer were calculated. In summer, the monoterpene, isoprene, toluene and β-caryophyllene SOA tracers accounted for 45.8%, 45.6%, 6.2% and 2.3% of the total SOA tracers, respectively. However, in winter, the percentages of monoterpene, isoprene, toluene and β-caryophyllene SOA tracers were 70.1%, 14.0%, 11.0% and 4.9%, respectively. The percentage of SOA_I tracers decreased sharply, due to the impacts of temperature on isoprene emissions, which was consisted with our previous findings (Hong et al., 2019). Meanwhile, the concentrations of SOA_M tracers were the largest in both seasons, due to a large amount of monoterpene emissions from the related plant species. Xiamen, an international garden city, located in coastal area of southeastern China. Monoterpene, such as α/β-pinene, is mostly emitted by coniferous plant and most flowers and fruits, while isoprene originates from broad-leaved trees and deciduous plants (Ding et al., 2014; Shrivastava et al., 2017; Yang et al., 2021).

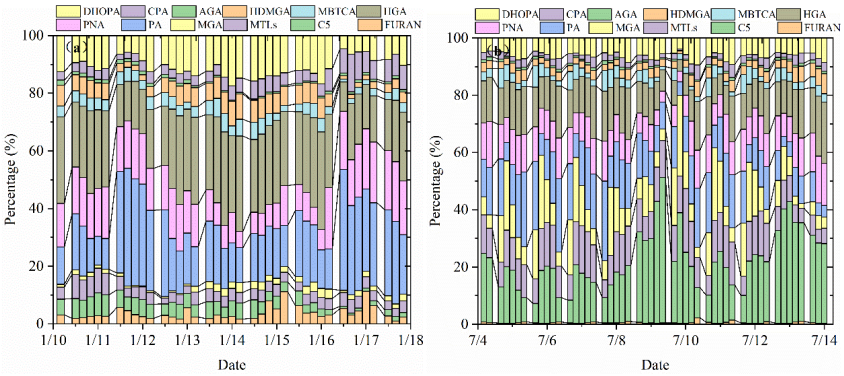

Figure 43. Percentages of isoprene, monoterpene, β-caryophyllene and toluene SOA tracers in winter (a) and summer (b)

The first (PA and PNA) and later generation (HGA, AGA, HDMGA and MBTCA) products were used to evaluate the aging degree of SOA_M (Ding et al., 2014; Hong et al., 2019). In this study, HGA (32.2%) was the major component of α/β-pinene tracers, followed by PA (30.5%), PNA (21.8%), HDMGA (7.3%), MBTCA (6.8%), and AGA (1.5%). The percentage of PA and PNA were much higher than those in mountainous background areas (PA: 9% and PNA: 3%)(Hong et al., 2019), suggesting the contribution of preliminary products to SOA in urban areas. As shown in Fig.43, the percentages of PA and PNA in winter (21.8% and 14.2%) were higher than those in summer (14.2% and 10.7%). Reacted with atmospheric oxidants including O_3 and OH, PA and PNA were transformed into MBTCA (Offenberg et al., 2007). This is the reason why the proportions of PA and PNA had a significant decreasing trend from winter to summer. The ratio of MBTCA/(PA+PNA) in summer and winter were 0.16±0.09 and 0.12±0.07, respectively, which also proved the impacts of atmospheric oxidation capacity on the aging degree of SOA_M. In addition, the ratio of HGA/MBTCA could be used to distinguish the contribution of α-pinene or β-pinene to the SOA_M formation (Jaoui et al., 2005; Ding et al., 2014). Low ratio of HGA/MBTCA (~1.0) showed that α-pinene was the major precursor for SOA_M (Lewandowski et al., 2013). The ratio of HGA/MBTCA with an average of 5.78 in Xiamen was high, suggesting the contribution

of β-pinene to SOA_M.

As shown in Fig.~~4~~3, MTLs and C5 alkene triols were the main components of the total SOA_I, with an average percentage of 68.0±14.9%, indicating a low-NOx environment (Ding et al., 2014; Liu et al., 2020). In summer, the percentages of MTLs and C5 alkene triols to the total SOA tracers in summer (21.8% and 14.2%) were obviously higher than those in winter (4.2% and 4.3%). This was consisted with the fact that the concentrations of NO_2 (14.8±7.46 μg m^{-3}) in summer was significantly lower than that (32.7±32.6 μg m^{-3}) in winter. Previous studies found that MTLs and C5 alkene triols were formed by the OH and HO_2 radicals via the HO_2 channel under low-NOx conditions (Surratt et al., 2010). C5 alkene triols are mainly produced by acid catalyzed reaction of Isoprene Epoxydiols (IEPOX) in the gas phase, while MTLs are formed by ring opening products of IEPOX (Surratt et al., 2007; Surratt et al., 2010). And the ozonolysis of isoprene was also an important pathway for MTLs in the presence of acid sulfate aerosols (Riva et al., 2016).

CPA, the typical tracer of sesquiterpenes, is formed by the photooxidation of β-caryophyllene (Jaoui et al., 2007). As shown in Fig.~~4~~3, CPA in winter and summer accounted for 5.0% and 2.3% of the total SOA tracers, respectively. This is because that the percentage of SOA_I has significant increase in summer. And the concentrations of CPA (2.5±2.0 ng m^{-3}) in summer were higher than that (1.7±0.8 ng m^{-3}) in winter, probably attributed to the emissions of β-caryophyllene driven by temperature and solar radiation. The CPA has a good correlation with DHOPA in summer (Fig.~~S2~~S4), suggesting the influence of photochemical oxidation (Liu et al., 2020). However, the CPA were not correlated with LEV in both seasons, reflecting the limited contribution of biomass burning (Zhang et al., 2019c).

3.4 Impacts of aerosol acidity on BSOA formation

Aerosol acidity (pH) was an important factor on SOA formation (Surratt et al., 2007; Offenberg et al., 2009; Zhang et al., 2019b; Zhang et al., 2019d). Time series of aerosol pH calculated by ISORROPIA II is shown in Fig.~~5~~4. The $PM_{2.5}$ in Xiamen was moderately acidic with daily pH range from 3.68 to 4.67. The highest aerosol pH was

observed in winter, and the lowest pH in summer. This is with similar seasonal trend, closing to the Yangtze River Delta (YRD) region, but obviously lower levels than those in NCP cities of China (Zhou et al., 2021). In general, the aerosol pH in Chinese cities were higher than those in US and European.

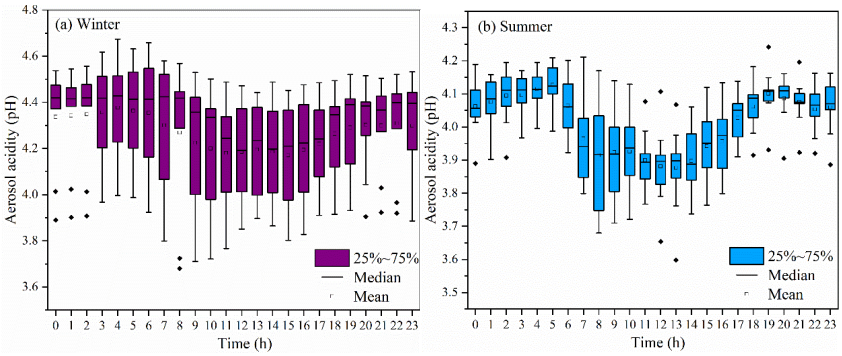

Figure ~~5~~4. Diurnal variations of aerosol acidity (pH) during the wintertime (a) and summertime (b) period (The boxes with error bars represent the 10th, 25th, 75th, and 90th percentiles)

A declining trend pH during the daytime was observed (Fig. ~~5~~4), which was related to the changes of chemical compositions and environmental conditions. The aerosol pH levels (~3 to 6) was related with a shift from sulfate- to nitrate-dominated aerosols (Guo et al., 2017). According to the multiphase buffer theory, the peak buffer pH (pKa*) regulated the aerosol pH, and temperature could obviously cause the variation of aerosol pH (Zheng et al., 2020). To further discuss the impacts of aerosol acidity on BSOA formation in coastal city, we analyzed the relationship between BSOA tracers and seed particles with different pH and liquid water content (LWC) (Fig. ~~S4~~ S5 and Table 1).

~~In Table 1, the BSOA tracers was linearly correlated with aerosol acidity (pH) and SO_4^{2-}. In summer, BSOA tracers in the particle phase were found to increase with increasing acidity, which was attributed to the presence of acid catalyzed aerosols. For example, isoprene SOA tracers is mainly formed through acid-catalyzed reactive uptake of isoprene-derived epoxydiols (IEPOX) onto sulfate aerosol particles.~~

Table 1 Correlations between individual BSOA tracer and environmental factors in winter and summer

Season	SOA tracer	pH	LWC	HONO	$PM_{2.5}$	Cl-	NO_3-	SO_4^{2-}	NH_3	SO_2	NO_2	Ox	T	RH	UV
WINTER (n=39)	C5	.584**	.701**	.534**	.690**	.569**	.710**	.663**	.705**	0.308	.353*	0.203	.361*	0.140	0.200
	MTLs	.590**	.705**	.431*	.665**	.639**	.707**	.651**	.757**	0.185	0.229	0.098	.353*	0.295	-0.068
	MGA	.390*	.707**	0.261	.668**	0.081	.758**	.572**	0.284	0.172	0.123	.374*	.377*	-0.019	0.238
	PA	.432*	.403**	.463**	.407**	.481*	.416*	.488*	.440*	.446*	0.241	-0.193	.319*	-0.205	0.145
	PNA	.489**	.579**	0.311	.459**	.516**	.573**	.533**	.543**	0.08	0.071	-0.101	0.121	.337*	-0.122
	HGA	.443*	.829**	.352*	.834**	.600**	.847**	.754**	.641**	0.275	0.299	.451**	.451**	0.043	0.210
	MBTCA	.433*	.678**	.447**	.670**	.435*	.733**	.589**	.710**	.327*	0.253	.492**	.552**	-0.158	0.317
	HDMGA	.421*	.876**	.401*	.867**	.631**	.884**	.813**	.643**	.335*	.321*	.526**	.485**	-0.049	0.327
	AGA	.570**	.575**	.370*	.488**	.577**	.566**	.544**	.731**	0.126	0.181	0.019	0.279	0.298	-0.122
	CPA	0.212	.462**	-0.068	.452**	.483**	.437*	.419*	0.255	-0.15	-0.170	0.016	0.079	0.200	-0.144
SUMMER (n=50)	C5	-.495**	.425**	0.160	.622**	-.340*	0.268	.625**	.436**	0.254	0.025	.649**	.573**	-.529**	0.247
	MTLs	-.551**	0.131	0.055	0.272	-.439**	0.131	.428**	.304*	0.089	-0.278	.550**	.610**	-.594**	0.263
	MGA	-.540**	0.029	0.116	0.132	-.403**	0.066	.472**	0.270	0.096	-.410**	.443**	.633**	-.668**	.382*
	PA	-.633**	.483**	.601**	.461**	-0.135	.541**	.502**	.405*	0.037	0.238	.456**	.626**	-.558**	.400*
	PNA	-.664**	.616**	.387**	.812**	-.389**	.450**	.784**	.503**	0.269	.294*	.769**	.718**	-.631**	.404*
	HGA	-.607**	.612**	.299*	.836**	-.384**	.447**	.770**	.539**	.316*	0.272	.808**	.670**	-.599**	0.322
	MBTCA	-.752**	.415**	0.237	.577**	-.382**	.359*	.636**	.501**	0.201	-0.052	.712**	.852**	-.816**	.588**
	HDMGA	-.525**	.618**	.299*	.833**	-.342*	.408**	.768**	.488**	.358*	.365**	.746**	.574**	-.500**	0.240
	AGA	-.684**	.592**	.447**	.766**	-.334*	.479**	.735**	.435**	0.244	0.271	.694**	.720**	-.634**	.477**
	CPA	-.552**	.625**	.441**	.780**	-.280*	.453**	.763**	.307*	.299*	.503**	.611**	.529**	-.458**	0.305

*/**Correlation coefficients with an asterisk indicate statistically significant relationships at a = 0.05, and two asterisks mean significant at a = 0.01.

In Table 1, the BSOA tracers was linearly correlated with aerosol acidity (pH) and SO_4^{2-}. In summer, BSOA tracers in the particle phase were found to increase with increasing acidity, which was attributed to the presence of acid catalyzed aerosols. For example, isoprene SOA tracers is mainly formed through acid-catalyzed reactive uptake of isoprene-derived epoxydiols (IEPOX) onto sulfate aerosol particles. In our previous studies, we have reported that high concentration of MTLs was related with sulfate, which could significantly promote the formation of isoprene-SOA tracers (Liu et al., 2020). Other studies also found that sulfate could increase the BSOA production by promoting acid-catalyzed ring-opening reactions (Xu et al., 2015). In contrast, positive correlations between BSOA tracers and aerosol pH in winter were observed, indicating that the formation of BSOA was predominantly enhanced by other factors, except for the aerosol acidity. The aerosol pH in winter was higher than those in summer, probably due to the influence of nitrate-dominated aerosols. Also, the aged aerosols through long-range transport might result in the increase of BSOA tracers and aerosol pH.

In addition, positive correlation between BSOA tracers and LWC was observed (Table 1), probably attributed to the effects of the LWC on determining the peak buffer pH (pKa*). Zheng et al. (2020) reported that the buffering effect of ammonia suppresses the contribution of different chemical compositions in aerosol particles, making LWC the primary determinant of aerosol pH. Other studies have demonstrated that the uptake coefficient of first-generation oxidation products, especially for carbonyl compounds, might depend on RH (Luo et al., 2019). Meanwhile, high LWC could reduce the aerosol particle viscosity, which was benefit to the generation of the reactive intermediate such as IEPOX, or other oxidation products of VOC into aqueous-phase of aerosol particles, thereby promoting the formation of BSOA (Zhang et al., 2019b; Zhang et al., 2019d).

3.5 Impacts of chlorine on BSOA formation

Halogen radicals (Cl, Br and I) originated from sea salt aerosol (SSA) have an important role in tropospheric oxidants chemistry (Wang et al., 2021c). In this study, chlorine depletion was frequently observed in summer (Fig.~~6b~~5b), indicating that HCl can be formed through acid displacement of sea salt aerosol Cl^- by H_2SO_4 and HNO_3 produced from anthropogenic emissions of SO_2 and NOx. Moreover, concentrations of the total SOA tracers were positively correlated with HCl (Fig.~~6a~~5a), suggesting the enhancement of SOA precursors transformation. Previous studies have found that Cl-initiated VOC oxidations could contribute to the formation of SOA (Wang and Ruiz,

带格式的：缩进：首行缩进： 0.85 厘米

2017; Dhulipala et al., 2019).

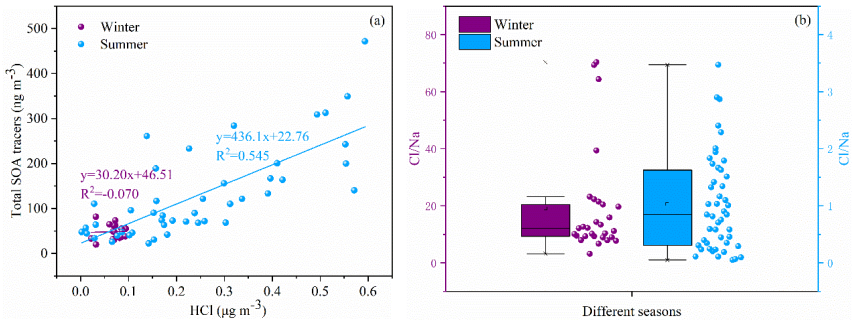

Figure ~~7~~6. Correlations of total SOA tracers and HCl (a) and chlorine depletion (b) in different seasons

Under ammonia-rich conditions, HCl partitioned into the aqueous particulate phase mostly took place, and chlorine ions could affect aqueous oxidation of secondary organic compounds (Xu et al., 2021). As shown in Table 1, most of SOA tracers in winter were correlated with the concentrations of chlorine ions in $PM_{2.5}$, while inverse results were observed in summer. In winter, the dominant wind direction is northeast (Fig.~~7~~6), and chlorine mainly come from continental polluted air mass, such as industrial and combustion emissions. So, anthropogenic pollutants through long-range transport might cause the enhancement of SOA tracer concentrations at the monitoring site. However, in summer, negative correlations of BSOA tracers and chlorine ions in $PM_{2.5}$ was found, probably due to the influence of chlorine depletion. As shown in Fig. ~~7~~6, the dominant wind direction is southerly, and chlorine mainly originated from the spray of sea salt.

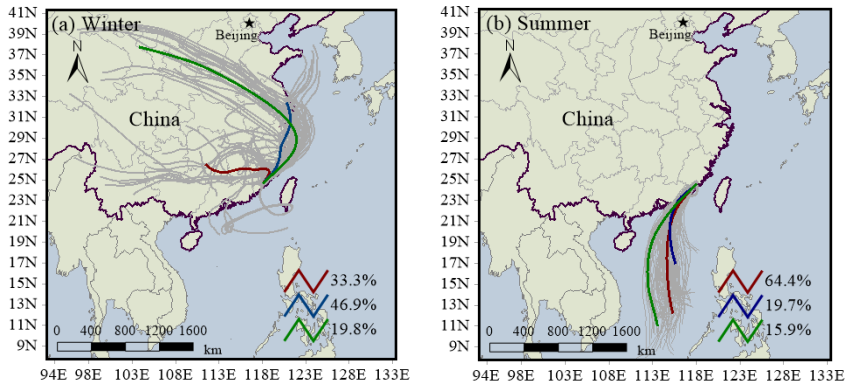

Figure ~~7~~6. Backward trajectories analyses during the winter (a) and summertime (b)

3.6. Enhanced formation of BSOA by anthropogenic emissions

Recent studies had indicated that anthropogenic emissions might affect SOA formation through multiple chemical processes, based on laboratory studies and field observations (Kari et al., 2019; Shrivastava et al., 2019; Zhang et al., 2019c; Cheng et al., 2021; Xu et al., 2021). In this study, we conducted the correlation analysis of individual SOA tracers and Ox (=O_3+NO_2), HONO, OH, SO_2, NH_3, $PM_{2.5}$, sulfate, nitrate, as well as meteorological parameters (including T, RH and UV) (Table 1).

Most of SOA tracers have a significant positive correlation with NH_3, suggesting an enhancement effect on the formation of SOA (Table 1). NH_3 could affect the SOA yields through both gas-phase and heterogeneous reactions (Na et al., 2007; Ma et al., 2018; Hao et al., 2020). Gas-phase reaction between NH_3 and organic acids (such as PA and PNA) produced ammonium salts in the particle phase, which contributed to the increased SOA formation. However, not all gas-phase organic acids (e.g., MGA and pyruvic acid) could demonstrate gas-to-particle conversion (Na et al., 2007). When SOA formation had ceased, the addition of excessive NH_3 would result in the rapid decomposition of the main SOA species, due to the nucleophilic attack of NH_3 (Ma et al., 2018).

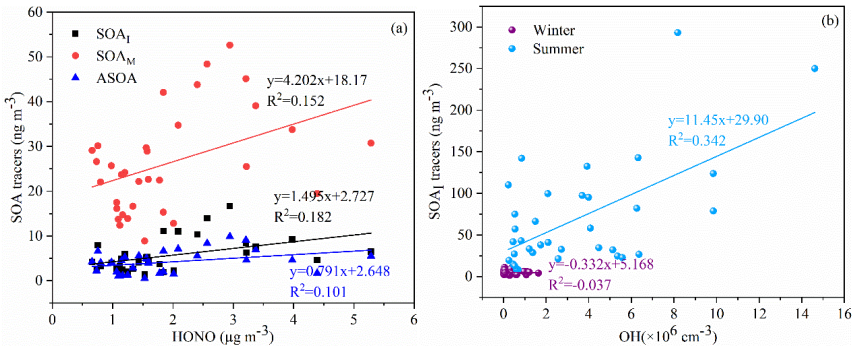

Figure ~~8~~7. Relationships of SOA tracers and HONO (a) and its estimated OH (b)

As an indicator of atmospheric oxidation capacity, the tropospheric odd oxygen Ox (O_3+NO_2) was calculated. As shown in Table 1, the majority of SOA tracers in summer showed significant positive correlations with Ox (R>0.5, P<0.001). However, in winter, a part of SOA_M tracers (e.g. HGA, MBTCA and HDMGA) were found to be significantly correlated with Ox. In addition, HONO and OH radicals, another critical indicator of atmospheric oxidation capacity, was also discussed. In this study, the concentration of OH radicals calculated from HONO in summer was higher than those in winter. In summer, the SOA_I tracers was correlated with OH radicals (Fig.~~8b~~7b), consisted with previous findings that OH radicals could promote the formation of SOA (Sarrafzadeh et al., 2016; Liu et al., 2019; Song et al., 2019; Zhang et al., 2019a). Due to its photolysis to produce OH radicals during the daytime, HONO could facilitate SOA formation. In winter, the concentrations of SOA_I, SOA_M and ASOA tracers were correlated with HONO (Fig.~~8a~~7a). These results indicated high concentrations of HONO and sufficient ultraviolet radiation could enhance the photochemical reactions of VOCs. Which was consisted with our previous results on the formation of peroxyacetyl nitrate (PAN) (Hu et al., 2020). As for T and UV, it exhibited significantly positive correlations with the related SOA tracers, especially in summer. These results suggested that SOA tracers were produced from the photo-oxidation of VOC precursors (Cheng et al., 2021).

In addition, the SOA tracers were significantly positive correlated with $PM_{2.5}$ and its components including NO_3- and SO_4^{2-}. In coastal cities of southeastern China, with the development of rapid urbanization, air pollution caused by motor vehicles and industrial emissions is becoming more frequent in winter (Wu et al., 2020). The Xiamen

port is one of the top 10 ports in China, resulting the impacts of ship emissions and port activities on ambient air quality (Xu et al., 2018), and the numbers of motor vehicles increased sharply in recent years. We also found that the 90th percentile of maximum daily average 8h (MDA8) O_3 concentrations in Xiamen was significantly increased from 2015 to 2020 (Fig. ~~S5~~S6). During the past several years, the elevated secondary inorganic components, including NO_3-, SO_4^{2-} and NH_4^+, accounted for 40-50% of the total $PM_{2.5}$, and OM ranged from 30% to 40% (Wu et al., 2019; Hong et al., 2021). These results also implied the effects of anthropogenic emissions and enhanced atmospheric oxidation capacity on secondary formation of aerosol particles under atmospheric stagnant conditions.

Conclusions

Pollution characteristics and source identification of BSOA tracers during the summer and winter in coastal areas of southeastern China were investigated. The average concentration of total BSOA tracers in summer was higher than that in winter, with the predominance of SOA_M, followed by SOA_I and SOA_C. The BSOA tracers in summer were predominantly produced by the influence of photochemical oxidation under relatively clean conditions. However, in winter, the formation of BSOA tracers were attributed to the impacts of anthropogenic emissions and atmospheric stagnant conditions. In addition, the results also indicated that acid-catalyzed reactive uptake onto sulfate aerosol particles enhanced the formation of BSOA in both seasons. We further found that Cl-initiated VOC oxidations has potentially accelerated the transformation of BSOA precursors through sea salt aerosol originated from the ocean in summer and anthropogenic emissions in winter. This study demonstrated that the combined effects of anthropogenic pollutants and atmospheric oxidation capacity on the formation of BSOA in coastal area.

Data Availability. The data set related to this work can be accessed via https://doi.org/10.5281/zenodo.6376025 (Hong, 2022). The details are also available upon request from the corresponding author (ywhong@iue.ac.cn).

Authorship Contribution Statement. Youwei Hong and Xinbei Xu contributed equally to this work. Youwei Hong designed and wrote the manuscript. Xinbei Xu collected the data, contributed to the data analysis. Dan Liao, Taotao Liu, Xiaoting Ji and Ke Xu

performed modeling analyses and data analysis. Jinsheng Chen supported funding of observation and research. Chunyang Liao, Ting Wang and Chunshui Lin contributed to revise the manuscript.

Competing interests. The authors declare that they have no conflict of interest.

Acknowledgement. The authors gratefully acknowledge Yanting Chen, Han Zhang and Xu Liao (Institute of Urban Environment, Chinese Academy of Sciences) for the guidance and assistance during sample pretreatment, and Lingling Xu and Mengren Li (Institute of Urban Environment, Chinese Academy of Sciences) for the discussion of this paper. This study was supported by Fujian Key Laboratory of Atmospheric Ozone Pollution Prevention and Xiamen Atmospheric Environment Observation and Research Station of Fujian Province (Institute of Urban Environment, Chinese Academy of Sciences).

Financial support. This research was financially supported by the Xiamen Youth Innovation Fund Project (3502Z20206094), the foreign cooperation project of Fujian Province (2020I0038), the Cultivating Project of Strategic Priority Research Program of Chinese Academy of Sciences (XDPB1903), the National Key Research and Development Program (2016YFC0112200), State Key Laboratory of Environmental Chemistry and Ecotoxicology, Research Center for Eco-Environmental Sciences, CAS (KF2020-06), the FJIRSM&IUE Joint Research Fund (RHZX-2019-006) and center for Excellence in Regional Atmospheric Environment project (E0L1B20201).

Reference

Charan, S. M., Huang, Y., and Seinfeld, J. H.: Computational Simulation of Secondary Organic Aerosol Formation in Laboratory Chambers, Chem. Rev., 119, 11912-11944, 10.1021/acs.chemrev.9b00358, 2019.

Cheng, Y., Ma, Y., and Hu, D.: Tracer-based source apportioning of atmospheric organic carbon and the influence of anthropogenic emissions on secondary organic aerosol formation in Hong Kong, Atmos. Chem. Phys., 21, 10589-10608, 10.5194/acp-21-10589-2021, 2021.

Dhulipala, S. V., Bhandari, S., and Hildebrandt Ruiz, L.: Formation of oxidized organic compounds from Cl-initiated oxidation of toluene, Atmospheric Environment, 199, 265-273, 10.1016/j.atmosenv.2018.11.002, 2019.

Ding, X., He, Q.-F., Shen, R.-Q., Yu, Q.-Q., and Wang, X.-M.: Spatial distributions of secondary organic aerosols from isoprene, monoterpenes, beta-caryophyllene, and

aromatics over China during summer, Journal of Geophysical Research-Atmospheres, 119, 11877-11891, 10.1002/2014jd021748, 2014.
Fountoukis, C., and Nenes, A.: ISORROPIA II: a computationally efficient thermodynamic equilibrium model for K^+–Ca^{2+}–Mg^{2+}–NH_4^+ –Na^+–SO_4^{2-} –NO_3^-–Cl^-–H_2O aerosols, Atmos. Chem. Phys., 7, 4639-4659, 10.5194/acp-7-4639-2007, 2007.
Fu, P., Kawamura, K., Chen, J., and Barrie, L. A.: Isoprene, Monoterpene, and Sesquiterpene Oxidation Products in the High Arctic Aerosols during Late Winter to Early Summer, Environmental Science & Technology, 43, 4022-4028, 10.1021/es803669a, 2009.
Guo, H., Sullivan, A. P., Campuzano-Jost, P., Schroder, J. C., Lopez-Hilfiker, F. D., Dibb, J. E., Jimenez, J. L., Thornton, J. A., Brown, S. S., Nenes, A., and Weber, R. J.: Fine particle pH and the partitioning of nitric acid during winter in the northeastern United States, Journal of Geophysical Research: Atmospheres, 121, 10,355-310,376, https://doi.org/10.1002/2016JD025311, 2016.
Guo, H., Weber, R. J., and Nenes, A.: High levels of ammonia do not raise fine particle pH sufficiently to yield nitrogen oxide-dominated sulfate production, Scientific Reports, 7, 12109, 10.1038/s41598-017-11704-0, 2017.
Hallquist, M., Wenger, J. C., Baltensperger, U., Rudich, Y., Simpson, D., Claeys, M., Dommen, J., Donahue, N. M., George, C., Goldstein, A. H., Hamilton, J. F., Herrmann, H., Hoffmann, T., Iinuma, Y., Jang, M., Jenkin, M. E., Jimenez, J. L., Kiendler-Scharr, A., Maenhaut, W., McFiggans, G., Mentel, T. F., Monod, A., Prevot, A. S. H., Seinfeld, J. H., Surratt, J. D., Szmigielski, R., and Wildt, J.: The formation, properties and impact of secondary organic aerosol: current and emerging issues, Atmospheric Chemistry and Physics, 9, 5155-5236, 10.5194/acp-9-5155-2009, 2009.
Hao, L., Kari, E., Leskinen, A., Worsnop, D. R., and Virtanen, A.: Direct contribution of ammonia to α-pinene secondary organic aerosol formation, Atmos. Chem. Phys., 20, 14393-14405, 10.5194/acp-20-14393-2020, 2020.
Hoffmann, D., Tilgner, A., Iinuma, Y., and Herrmann, H.: Atmospheric Stability of Levoglucosan: A Detailed Laboratory and Modeling Study, Environmental Science & Technology, 44, 694-699, 10.1021/es902476f, 2010.
Hong, Y., Xu, X., Liao, D., Zheng, R., Ji, X., Chen, Y., Xu, L., Li, M., Wang, H., Xiao, H., Choi, S.-D., and Chen, J.: Source apportionment of PM2.5 and sulfate formation during the COVID-19 lockdown in a coastal city of southeast China, Environmental Pollution, 286, 117577, https://doi.org/10.1016/j.envpol.2021.117577, 2021.
Hong, youwei. (2022). Dataset for ACP by Hong et al., 2022 [Data set]. Zenodo. https://doi.org/10.5281/zenodo.6376025
Hong, Z., Zhang, H., Zhang, Y., Xu, L., Liu, T., Xiao, H., Hong, Y., Chen, J., Li, M., Deng, J., Wu, X., Hu, B., and Chen, X.: Secondary organic aerosol of PM2.5 in a mountainous forest area in southeastern China: Molecular compositions and tracers implication, Science of the Total Environment, 653, 496-503, 10.1016/j.scitotenv.2018.10.370, 2019.
Hoyle, C. R., Boy, M., Donahue, N. M., Fry, J. L., Glasius, M., Guenther, A., Hallar, A. G., Hartz, K. H., Petters, M. D., Petaja, T., Rosenoern, T., and Sullivan, A. P.: A review of the anthropogenic influence on biogenic secondary organic aerosol, Atmospheric Chemistry and Physics, 11, 321-343, 10.5194/acp-11-321-2011, 2011.
Hu, B., Liu, T., Hong, Y., Xu, L., Li, M., Wu, X., Wang, H., Chen, J., and Chen, J.: Characteristics of peroxyacetyl nitrate (PAN) in a coastal city of southeastern China: Photochemical mechanism and pollution process, Science of the Total Environment, 719, 10.1016/j.scitotenv.2020.137493, 2020.
Hu, W., Palm, B. B., Day, D. A., Campuzano-Jost, P., Krechmer, J. E., Peng, Z., de Sa, S. S., Martin, S. T., Alexander, M. L., Baumann, K., Hacker, L., Kiendler-Scharr, A., Koss, A. R., de Gouw, J. A., Goldstein, A. H., Seco, R., Sjostedt, S. J., Park, J.-H., Guenther, A. B., Kim, S., Canonaco, F., Prevot, A. S. H., Brune, W. H., and Jimenez, J. L.: Volatility

and lifetime against OH heterogeneous reaction of ambient isoprene-epoxydiols-derived secondary organic aerosol (IEPOX-SOA), Atmospheric Chemistry and Physics, 16, 11563-11580, 10.5194/acp-16-11563-2016, 2016.

Jaoui, M., Kleindienst, T. E., Lewandowski, M., Offenberg, J. H., and Edney, E. O.: Identification and quantification of aerosol polar oxygenated compounds bearing carboxylic or hydroxyl groups. 2. Organic tracer compounds from monoterpenes, Environmental Science & Technology, 39, 5661-5673, 10.1021/es048111b, 2005.

Jaoui, M., Lewandowski, M., Kleindienst, T. E., Offenberg, J. H., and Edney, E. O.: β-caryophyllinic acid: An atmospheric tracer forβ-caryophyllene secondary organic aerosol, Geophysical Research Letters, 34, 10.1029/2006gl028827, 2007.

Kari, E., Hao, L. Q., Ylisirnio, A., Buchholz, A., Leskinen, A., Yli-Pirila, P., Nuutinen, I., Kuuspalo, K., Jokiniemi, J., Faiola, C. L., Schobesberger, S., and Virtanen, A.: Potential dual effect of anthropogenic emissions on the formation of biogenic secondary organic aerosol (BSOA), Atmospheric Chemistry and Physics, 19, 15651-15671, 10.5194/acp-19-15651-2019, 2019.

Kleindienst, T. E., Jaoui, M., Lewandowski, M., Offenberg, J. H., Lewis, C. W., Bhave, P. V., and Edney, E. O.: Estimates of the contributions of biogenic and anthropogenic hydrocarbons to secondary organic aerosol at a southeastern US location, Atmospheric Environment, 41, 8288-8300, 10.1016/j.atmosenv.2007.06.045, 2007.

Lewandowski, M., Piletic, I. R., Kleindienst, T. E., Offenberg, J. H., Beaver, M. R., Jaoui, M., Docherty, K. S., and Edney, E. O.: Secondary organic aerosol characterisation at field sites across the United States during the spring-summer period, International Journal of Environmental Analytical Chemistry, 93, 1084-1103, 10.1080/03067319.2013.803545, 2013.

Liu, S., Tsona, N. T., Zhang, Q., Jia, L., Xu, Y., and Du, L.: Influence of relative humidity on cyclohexene SOA formation from OH photooxidation, Chemosphere, 231, 478-486, 10.1016/j.chemosphere.2019.05.131, 2019.

Liu, S., Huang, D., Wang, Y., Zhang, S., Wu, C., Du, W., and Wang, G.: Synergetic effect of NH_3 and NOx on the production and optical absorption of secondary organic aerosol formation from toluene photooxidation, Atmos. Chem. Phys. Discuss., 2021, 1-38, 10.5194/acp-2021-560, 2021.

Liu, T., Hu, B., Xu, X., Hong, Y., Zhang, Y., Wu, X., Xu, L., Li, M., Chen, Y., Chen, X., and Chen, J.: Characteristics of PM2.5-bound secondary organic aerosol tracers in a coastal city in Southeastern China: Seasonal patterns and pollution identification, Atmospheric Environment, 237, 10.1016/j.atmosenv.2020.117710, 2020.

Lopez-Hilfiker, F. D., Mohr, C., D'Ambro, E. L., Lutz, A., Riedel, T. P., Gaston, C. J., Iyer, S., Zhang, Z., Gold, A., Surratt, J. D., Lee, B. H., Kurten, T., Hu, W. W., Jimenez, J., Hallquist, M., and Thornton, J. A.: Molecular Composition and Volatility of Organic Aerosol in the Southeastern US: Implications for IEPDX Derived SOA, Environmental Science & Technology, 50, 2200-2209, 10.1021/acs.est.5b04769, 2016.

Lowes, S., Jersey, J., Shoup, R., Garofolo, F., Savoie, N., Mortz, E., Needham, S., Caturla, M. C., Steffen, R., Sheldon, C., Hayes, R., Samuels, T., Di Donato, L., Kamerud, J., Michael, S., Lin, Z. P., Hillier, J., Moussallie, M., Teixeira, L. D., Rocci, M., Buonarati, M., Truog, J., Hussain, S., Lundberg, R., Breau, A., Zhang, T. Y., Jonker, J., Berger, N., Gagnon-Carignan, S., Nehls, C., Nicholson, R., Hilhorst, M., Karnik, S., de Boer, T., Houghton, R., Smith, K., Cojocaru, L., Allen, M., Harter, T., Fatmi, S., Sayyarpour, F., Vija, J., Malone, M., and Heller, D.: Recommendations on: internal standard criteria, stability, incurred sample reanalysis and recent 483s by the Global CRO Council for Bioanalysis, Bioanalysis, 3, 1323-1332, 10.4155/Bio.11.135, 2011.

Luo, H., Jia, L., Wan, Q., An, T., and Wang, Y.: Role of liquid water in the formation of O-3 and SOA particles from 1,2,3-trimethylbenzene, Atmospheric Environment, 217, 10.1016/j.atmosenv.2019.116955, 2019.

Lv, S., Wang, F., Wu, C., Chen, Y., Liu, S., Zhang, S., Li, D., Du, W., Zhang, F., Wang, H., Huang, C., Fu, Q., Duan, Y., and Wang, G.: Gas-to-Aerosol Phase Partitioning of Atmospheric Water-Soluble Organic Compounds at a Rural Site in China: An Enhancing Effect of NH3 on SOA Formation, Environmental Science & Technology, 10.1021/acs.est.1c06855, 2022.
Ma, Q., Lin, X. X., Yang, C. G., Long, B., Gai, Y. B., and Zhang, W. J.: The influences of ammonia on aerosol formation in the ozonolysis of styrene: roles of Criegee intermediate reactions, Roy Soc Open Sci, 5, ARTN 17217110.1098/rsos.172171, 2018.
Mahilang, M., Deb, M. K., and Pervez, S.: Biogenic secondary organic aerosols: A review on formation mechanism, analytical challenges and environmental impacts, Chemosphere, 262, 10.1016/j.chemosphere.2020.127771, 2021.
McFiggans, G., Mentel, T. F., Wildt, J., Pullinen, I., Kang, S., Kleist, E., Schmitt, S., Springer, M., Tillmann, R., Wu, C., Zhao, D. F., Hallquist, M., Faxon, C., Le Breton, M., Hallquist, A. M., Simpson, D., Bergstrom, R., Jenkin, M. E., Ehn, M., Thornton, J. A., Alfarra, M. R., Bannan, T. J., Percival, C. J., Priestley, M., Topping, D., and Kiendler-Scharr, A.: Secondary organic aerosol reduced by mixture of atmospheric vapours, Nature, 565, 587-593, 10.1038/s41586-018-0871-y, 2019.
Na, K., Song, C., Switzer, C., and Cocker, D. R.: Effect of Ammonia on Secondary Organic Aerosol Formation from α-Pinene Ozonolysis in Dry and Humid Conditions, Environmental Science & Technology, 41, 6096-6102, 10.1021/es061956y, 2007.
Newland, M. J., Bryant, D. J., Dunmore, R. E., Bannan, T. J., Acton, W. J. F., Langford, B., Hopkins, J. R., Squires, F. A., Dixon, W., Drysdale, W. S., Ivatt, P. D., Evans, M. J., Edwards, P. M., Whalley, L. K., Heard, D. E., Slater, E. J., Woodward-Massey, R., Ye, C., Mehra, A., Worrall, S. D., Bacak, A., Coe, H., Percival, C. J., Hewitt, C. N., Lee, J. D., Cui, T., Surratt, J. D., Wang, X., Lewis, A. C., Rickard, A. R., and Hamilton, J. F.: Low-NO atmospheric oxidation pathways in a polluted megacity, Atmos. Chem. Phys., 21, 1613-1625, 10.5194/acp-21-1613-2021, 2021.
Offenberg, J. H., Lewis, C. W., Lewandowski, M., Jaoui, M., Kleindienst, T. E., and Edney, E. O.: Contributions of toluene and alpha-pinene to SOA formed in an irradiated toluene/alpha-pinene/NOx/air mixture: Comparison of results using C-14 content and SOA organic tracer methods, Environmental Science & Technology, 41, 3972-3976, 10.1021/es070089+, 2007.
Offenberg, J. H., Lewandowski, M., Edney, E. O., Kleindienst, T. E., and Jaoui, M.: Influence of Aerosol Acidity on the Formation of Secondary Organic Aerosol from Biogenic Precursor Hydrocarbons, Environmental Science & Technology, 43, 7742-7747, 10.1021/es901538e, 2009.
Palmer, P. I., Marvin, M. R., Siddans, R., Kerridge, B. J., and Moore, D. P.: Nocturnal survival of isoprene linked to formation of upper tropospheric organic aerosol, Science, 375, 562-566, doi:10.1126/science.abg4506, 2022.
Reid, J. P., Bertram, A. K., Topping, D. O., Laskin, A., Martin, S. T., Petters, M. D., Pope, F. D., and Rovelli, G.: The viscosity of atmospherically relevant organic particles, Nature Communications, 9, 10.1038/s41467-018-03027-z, 2018.
Riva, M., Budisulistiorini, S. H., Zhang, Z., Gold, A., and Surratt, J. D.: Chemical characterization of secondary organic aerosol constituents from isoprene ozonolysis in the presence of acidic aerosol, Atmospheric Environment, 130, 5-13, 10.1016/j.atmosenv.2015.06.027, 2016.
Rumsey, I. C., Cowen, K. A., Walker, J. T., Kelly, T. J., Hanft, E. A., Mishoe, K., Rogers, C., Proost, R., Beachley, G. M., Lear, G., Frelink, T., and Otjes, R. P.: An assessment of the performance of the Monitor for AeRosols and GAses in ambient air (MARGA): a semi-continuous method for soluble compounds, Atmos. Chem. Phys., 14, 5639-5658, 10.5194/acp-14-5639-2014, 2014.
Sarrafzadeh, M., Wildt, J., Pullinen, I., Springer, M., Kleist, E., Tillmann, R., Schmitt, S. H., Wu, C., Mentel, T. F., Zhao, D., Hastie, D. R., and Kiendler-Scharr, A.: Impact of NOx

723 and OH on secondary organic aerosol formation from beta-pinene photooxidation,
724 Atmospheric Chemistry and Physics, 16, 11237-11248, 10.5194/acp-16-11237-2016,
725 2016.
726 Shrivastava, M., Cappa, C. D., Fan, J., Goldstein, A. H., Guenther, A. B., Jimenez, J. L.,
727 Kuang, C., Laskin, A., Martin, S. T., Ng, N. L., Petaja, T., Pierce, J. R., Rasch, P. J.,
728 Roldin, P., Seinfeld, J. H., Shilling, J., Smith, J. N., Thornton, J. A., Volkamer, R.,
729 Wang, J., Worsnop, D. R., Zaveri, R. A., Zelenyuk, A., and Zhang, Q.: Recent advances
730 in understanding secondary organic aerosol: Implications for global climate forcing,
731 Reviews of Geophysics, 55, 509-559, 10.1002/2016rg000540, 2017.
732 Shrivastava, M., Andreae, M. O., Artaxo, P., Barbosa, H. M. J., Berg, L. K., Brito, J., Ching,
733 J., Easter, R. C., Fan, J., Fast, J. D., Feng, Z., Fuentes, J. D., Glasius, M., Goldstein, A.
734 H., Alves, E. G., Gomes, H., Gu, D., Guenther, A., Jathar, S. H., Kim, S., Liu, Y., Lou,
735 S., Martin, S. T., McNeill, V. F., Medeiros, A., de Sa, S. S., Shilling, J. E., Springston, S.
736 R., Souza, R. A. F., Thornton, J. A., Isaacman-VanWertz, G., Yee, L. D., Ynoue, R.,
737 Zaveri, R. A., Zelenyuk, A., and Zhao, C.: Urban pollution greatly enhances formation of
738 natural aerosols over the Amazon rainforest, Nature Communications, 10,
739 10.1038/s41467-019-08909-4, 2019.
740 Song, M., Zhang, C., Wu, H., Mu, Y., Ma, Z., Zhang, Y., Liu, J., and Li, X.: The influence of
741 OH concentration on SOA formation from isoprene photooxidation, Science of the Total
742 Environment, 650, 951-957, 10.1016/j.scitotenv.2018.09.084, 2019.
743 Surratt, J. D., Lewandowski, M., Offenberg, J. H., Jaoui, M., Kleindienst, T. E., Edney, E. O.,
744 and Seinfeld, J. H.: Effect of acidity on secondary organic aerosol formation from
745 isoprene, Environmental Science & Technology, 41, 5363-5369, 10.1021/es0704176,
746 2007.
747 Surratt, J. D., Chan, A. W. H., Eddingsaas, N. C., Chan, M., Loza, C. L., Kwan, A. J., Hersey,
748 S. P., Flagan, R. C., Wennberg, P. O., and Seinfeld, J. H.: Reactive intermediates
749 revealed in secondary organic aerosol formation from isoprene, Proceedings of the
750 National Academy of Sciences of the United States of America, 107, 6640-6645,
751 10.1073/pnas.0911114107, 2010.
752 Wang, D. S., and Ruiz, L. H.: Secondary organic aerosol from chlorine-initiated oxidation of
753 isoprene, Atmos. Chem. Phys., 17, 13491-13508, 10.5194/acp-17-13491-2017, 2017.
754 Wang, J., Ye, J., Zhang, Q., Zhao, J., Wu, Y., Li, J., Liu, D., Li, W., Zhang, Y., Wu, C., Xie,
755 C., Qin, Y., Lei, Y., Huang, X., Guo, J., Liu, P., Fu, P., Li, Y., Lee, H. C., Choi, H.,
756 Zhang, J., Liao, H., Chen, M., Sun, Y., Ge, X., Martin, S. T., and Jacob, D. J.: Aqueous
757 production of secondary organic aerosol from fossil-fuel emissions in winter Beijing
758 haze, Proc Natl Acad Sci U S A, 118, 10.1073/pnas.2022179118, 2021a.
759 Wang, J., Ye, J., Zhang, Q., Zhao, J., Wu, Y., Li, J., Liu, D., Li, W., Zhang, Y., Wu, C., Xie,
760 C., Qin, Y., Lei, Y., Huang, X., Guo, J., Liu, P., Fu, P., Li, Y., Lee, H. C., Choi, H.,
761 Zhang, J., Liao, H., Chen, M., Sun, Y., Ge, X., Martin, S. T., and Jacob, D. J.: Aqueous
762 production of secondary organic aerosol from fossil-fuel emissions in winter Beijing
763 haze, Proceedings of the National Academy of Sciences of the United States of America,
764 118, 10.1073/pnas.2022179118, 2021b.
765 Wang, S., Du, L., Tsona, N. T., Jiang, X., You, B., Xu, L., Yang, Z., and Wang, W.: Effect of
766 NOx and SO2 on the photooxidation of methylglyoxal: Implications in secondary
767 aerosol formation, J Environ Sci (China), 92, 151-162, 10.1016/j.jes.2020.02.011, 2020.
768 Wang, X., Jacob, D. J., Downs, W., Zhai, S., Zhu, L., Shah, V., Holmes, C. D., Sherwen, T.,
769 Alexander, B., Evans, M. J., Eastham, S. D., Neuman, J. A., Veres, P. R., Koenig, T. K.,
770 Volkamer, R., Huey, L. G., Bannan, T. J., Percival, C. J., Lee, B. H., and Thornton, J. A.:
771 Global tropospheric halogen (Cl, Br, I) chemistry and its impact on oxidants, Atmos.
772 Chem. Phys., 21, 13973-13996, 10.5194/acp-21-13973-2021, 2021c.
773 Wen, L., Chen, T., Zheng, P., Wu, L., Wang, X., Mellouki, A., Xue, L., and Wang, W.:
774 Nitrous acid in marine boundary layer over eastern Bohai Sea, China: Characteristics,
775 sources, and implications, Sci. Total Environ., 10.1016/j.scitotenv.2019.03.225, 2019.

776 Wu, X., Xu, L. L., Hong, Y. W., Chen, J. F., Qiu, Y. Q., Hu, B. Y., Hong, Z. Y., Zhang, Y.
777 R., Liu, T. T., Chen, Y. T., Bian, Y. H., Zhao, G. Q., Chen, J. S., and Li, M. R.: The air
778 pollution governed by subtropical high in a coastal city in Southeast China: Formation
779 processes and influencing mechanisms, Science of the Total Environment, 692, 1135-
780 1145, 10.1016/j.scitotenv.2019.07.341, 2019.
781 Wu, X., Li, M., Chen, J., Wang, H., Xu, L., Hong, Y., Zhao, G., Hu, B., Zhang, Y., Dan, Y.,
782 and Yu, S.: The characteristics of air pollution induced by the quasi-stationary front:
783 Formation processes and influencing factors, Science of the Total Environment, 707,
784 10.1016/j.scitotenv.2019.136194, 2020.
785 Xiao, Y., Wu, Z., Guo, S., He, L., Huang, X., and Hu, M.: Formation mechanism of
786 secondary organic aerosol in aerosol liquid water:A review, Chinese Science Bulletin,
787 65, 3118-3133, 2020.
788 Xu, L., Du, L., Tsona, N. T., and Ge, M. F.: Anthropogenic Effects on Biogenic Secondary
789 Organic Aerosol Formation, Advances in Atmospheric Sciences, 38, 1053-1084,
790 10.1007/s00376-020-0284-3, 2021.
791 Xu, L., Guo, H. Y., Boyd, C. M., Klein, M., Bougiatioti, A., Cerully, K. M., Hite, J. R.,
792 Isaacman-VanWertz, G., Kreisberg, N. M., Knote, C., Olson, K., Koss, A., Goldstein, A.
793 H., Hering, S. V., de Gouw, J., Baumann, K., Lee, S. H., Nenes, A., Weber, R. J., and
794 Ng, N. L.: Effects of anthropogenic emissions on aerosol formation from isoprene and
795 monoterpenes in the southeastern United States, Proceedings of the National Academy of
796 Sciences of the United States of America, 112, 37-42, 10.1073/pnas.1417609112, 2015.
797 Yang, W., Cao, J., Wu, Y., Kong, F., and Li, L.: Review on plant terpenoid emissions
798 worldwide and in China, The Science of the total environment, 787, 147454-147454,
799 10.1016/j.scitotenv.2021.147454, 2021.
800 Zhang, J., An, J., Qu, Y., Liu, X., and Chen, Y.: Impacts of potential HONO sources on the
801 concentrations of oxidants and secondary organic aerosols in the Beijing-Tianjin-Hebei
802 region of China, Science of the Total Environment, 647, 836-852,
803 10.1016/j.scitotenv.2018.08.030, 2019a.
804 Zhang, P., Chen, T., Liu, J., Liu, C., Ma, J., Ma, Q., Chu, B., and He, H.: Impacts of SO2,
805 Relative Humidity, and Seed Acidity on Secondary Organic Aerosol Formation in the
806 Ozonolysis of Butyl Vinyl Ether, Environmental Science & Technology, 53, 8845-8853,
807 10.1021/acs.est.9b02702, 2019b.
808 Zhang, Y.-Q., Chen, D.-H., Ding, X., Li, J., Zhang, T., Wang, J.-Q., Cheng, Q., Jiang, H.,
809 Song, W., Ou, Y.-B., Ye, P.-L., Zhang, G., and Wang, X.-M.: Impact of anthropogenic
810 emissions on biogenic secondary organic aerosol: observation in the Pearl River Delta,
811 southern China, Atmospheric Chemistry and Physics, 19, 14403-14415, 10.5194/acp-19-
812 14403-2019, 2019c.
813 Zhang, Y., Chen, Y., Lei, Z., Olson, N. E., Riva, M., Koss, A. R., Zhang, Z., Gold, A., Jayne,
814 J. T., Worsnop, D. R., Onasch, T. B., Kroll, J. H., Turpin, B. J., Ault, A. P., and Surratt,
815 J. D.: Joint Impacts of Acidity and Viscosity on the Formation of Secondary Organic
816 Aerosol from Isoprene Epoxydiols (IEPDX) in Phase Separated Particles, Acs Earth and
817 Space Chemistry, 3, 2646-2658, 10.1021/acsearthspacechem.9b00209, 2019d.
818 Zhao, D. F., Schmitt, S. H., Wang, M. J., Acir, I. H., Tillmann, R., Tan, Z. F., Novelli, A.,
819 Fuchs, H., Pullinen, I., Wegener, R., Rohrer, F., Wildt, J., Kiendler-Scharr, A., Wahner,
820 A., and Mentel, T. F.: Effects of NOx and SO2 on the secondary organic aerosol
821 formation from photooxidation of alpha-pinene and limonene, Atmospheric Chemistry
822 and Physics, 18, 1611-1628, 10.5194/acp-18-1611-2018, 2018.
823 Zheng, G., Su, H., Wang, S., Andreae, M. O., Poschl, U., and Cheng, Y.: Multiphase buffer
824 theory explains contrasts in atmospheric aerosol acidity, Science, 369, 1374-+,
825 10.1126/science.aba3719, 2020.
826 Zhou, M., Zheng, G., Wang, H., Qiao, L., Zhu, S., Huang, D., An, J., Lou, S., Tao, S., Wang,
827 Q., Yan, R., Ma, Y., Chen, C., Cheng, Y., Su, H., and Huang, C.: Long-term trends and

drivers of aerosol pH in eastern China, Atmos. Chem. Phys. Discuss., 2021, 1-21, 10.5194/acp-2021-455, 2021.
Zhu, J., Penner, J. E., Yu, F., Sillman, S., Andreae, M. O., and Coe, H.: Decrease in radiative forcing by organic aerosol nucleation, climate, and land use change, Nature Communications, 10, 10.1038/s41467-019-08407-7, 2019.